ELSEVIER

Combustion and Flame 135 (2003) 381–403

Combustion and Flame

Hydroxyl time-series measurements and simulations for turbulent premixed jet flames in the thickened preheat regime

Walter A. Guttenfelder[a], Galen B. King[a], Jay P. Gore[a], Normand M. Laurendeau[a], Michael W. Renfro[b,*]

[a]*School of Mechanical Engineering, Purdue University, West Lafayette, IN 47907-1288, USA*
[b]*Mechanical Engineering Department, University of Connecticut, Storrs, CT 06269-3139, USA*

Received 18 December 2001; received in revised form 22 April 2003; accepted 1 July 2003

Abstract

Quantitative measurements of OH concentration time series are presented for turbulent lean-premixed, methane-air jet flames theoretically in the thickened preheat regime. Picosecond time-resolved laser-induced fluorescence (PITLIF) reveals unique differences between these premixed flames and previous non-premixed jet flames. Time-averaged [OH] measurements are used to identify mean flame structures and to discern how these structures are affected by varying bulk flow velocities and heat release. More importantly, hydroxyl time series are inspected to distinguish among three main regions in these turbulent premixed flames. These regions include the reacting side of the flame brush, the mixing side of the flame brush (radially outside the location of heat release), and above the flame tip. Although the main reaction zone appears to be broadened by its associated high turbulent intensity, a combination of statistical analysis plus flamelet simulations suggests that the primary internal structure responsible for the OH distribution remains constant across the mean flame brush. Therefore, the absolute concentration of OH depends principally on the intermittency of this instantaneous internal structure. Outside the mean flame brush, mixing of OH with co-flow air shifts the distribution of absolute OH concentrations. Distinct autocorrelation functions are found within the three different regions identified for these premixed flames. Across the flame brush, integral time scales are dominated by turbulent convection, as verified by flamelet simulations. Above the flame tip, integral time scales are determined by a competition between turbulent convection and the reaction rate for OH destruction.

Keywords: Hydroxyl time series; Turbulent premixed flames; Integral time scales

1. Introduction

Studies of turbulent lean-premixed flames are important as they provide an opportunity for reduced emissions because of lower instantaneous flame temperatures as compared to those in non-premixed flames. Classically, turbulent premixed-flame regimes have been developed to distinguish among different fundamental turbulence-chemistry interactions, which are important not only in understanding the underlying physics of such flames, but also in creating the required models to predict flame characteristics. Damköhler [1] originally proposed two regimes based on either coarse-body turbulence with small velocity fluctuations or fine-body turbulence

* Corresponding author: Tel.: 765-494-2713; fax: 765-494-0539.

E-mail address: laurende@ecn.purdue.edu (N. Laurendeau).

0010-2180/03/$ – see front matter
doi:10.1016/S0010-2180(03)00184-6

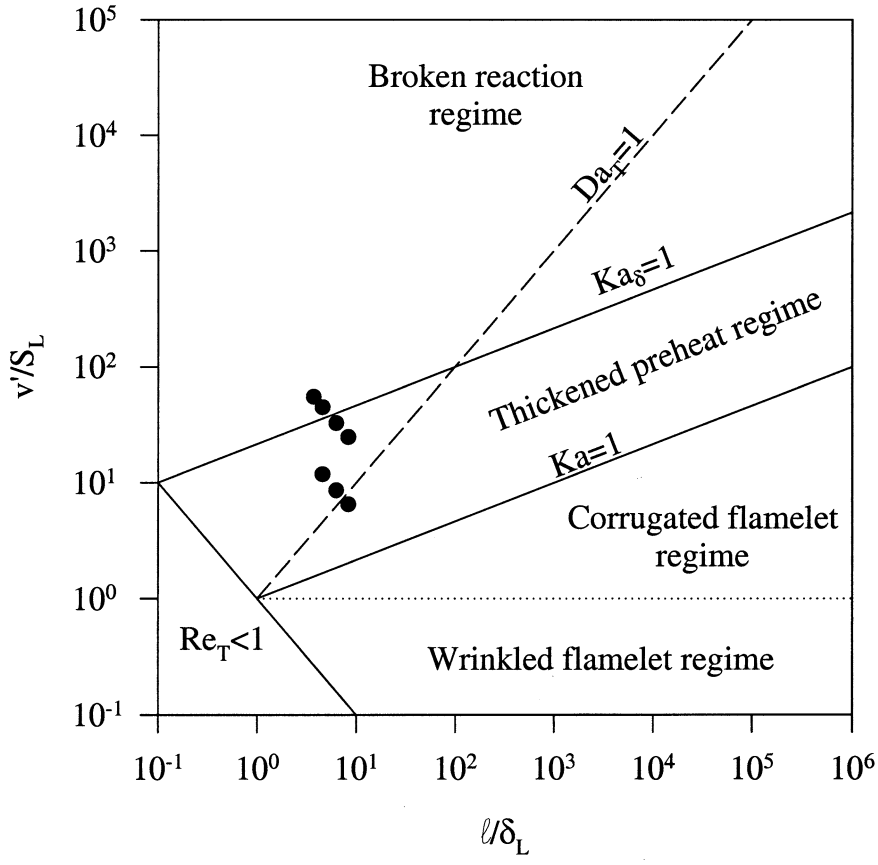

Fig. 1. Turbulent premixed flame regimes based on a ratio of the turbulent integral length scale to laminar flame thickness, ℓ/δ_L, and rms turbulent velocity to laminar flame speed, v'/S_L. Lines of unity dimensionless parameters are also shown, as they are used in separating the different combustion regimes, e.g., $\mathrm{Re_T} = 1$, $\mathrm{Da_T} = 1$, and $\mathrm{Ka} = 1$. The data points indicate the flames of this investigation, which mostly occur theoretically within the thickened preheat regime.

with large velocity fluctuations, using a ratio of mixing length scale for the turbulence, ℓ, and the laminar flame thickness, δ_L, to separate the two regimes. More recently, regime diagrams have been created based on dimensionless parameters, such as the turbulent Damköhler and Reynolds numbers [2], and on ratios of both length scales (ℓ/δ_L) and velocity scales (v'/S_L) [3–5], where v' is the rms of the fluctuating velocity and S_L is the laminar flame speed. The turbulent Damköhler and Reynolds numbers are defined as

$$\mathrm{Da_T} = \frac{t_f}{t_c} = \frac{\ell/v'}{\delta_L/S_L} \tag{1}$$

$$\mathrm{Re_T} = \frac{v'\ell}{\nu} \tag{2}$$

where, t_f is a characteristic flow time, often associated with an eddy turn-over time, t_c is a characteristic chemical time scale, and ν is the kinematic viscosity of the gas mixture. The flame thickness, δ_L, is determined using the thermal diffusivity and laminar flame speed via

$$\delta_\mathrm{L} = \frac{\alpha}{S_L}. \tag{3}$$

Figure 1 provides one example of a regime chart most recently proposed by Peters [5]. For low-intensity turbulence ($v'/S_\mathrm{L} < 1$), wrinkled flamelets are hypothesized to exist, analogous to Damköhler's coarse-body turbulence and independent of the turbulent length scale. For increasing turbulent intensities ($v'/S_\mathrm{L} > 1$), the flame surface distorts sufficiently to create multiply connected flamelets that can surround pockets of unburned reactants. This behavior corresponds to the corrugated flamelet regime. As turbulence intensities increase further, a new threshold is met, classically represented by the Klimov-

Williams (K-W) criterion. This criterion is based on the product of the highest significant strain rate with the residence time in the flame [6]. If the strain rate is represented by the inverse of a Kolmogorov eddy time, t_k, and the residence time in the flame by $t_c = \delta_L/S_L$, the K-W criterion can be expressed using Eq. 3 in terms of the Karlovitz number

$$\mathrm{Ka} = \frac{t_c}{t_k} = \frac{\delta_L^2}{\ell_k^2} = \frac{\upsilon_k^2}{S_L^2}, \tag{4}$$

where the Kolmogorov length, ℓ_k, time, t_k, and velocity, υ_k, scales are given by [7]

$$\ell_k = \left(\frac{\nu^3}{\varepsilon}\right)^{1/4} \quad t_k = \left(\frac{\nu}{\varepsilon}\right)^{1/2} \quad \upsilon_k = (\nu\varepsilon)^{1/4} \tag{5}$$

for which $\varepsilon = \nu'^3/\ell$ is the turbulence dissipation rate. A flamelet structure is hypothesized to exist in premixed flames if $\mathrm{Ka} < 1$. When $\mathrm{Ka} > 1$, the reaction is classically hypothesized to exist in the distributed reaction regime [3,4], where the smallest eddies can enter into and broaden the flame structure.

An additional regime can be identified wherein the smallest turbulent eddies lie between the overall flame width, δ_L which includes the preheat zone, and the actual reaction-zone width [3]. For this case, small energetic eddies are hypothesized to penetrate and broaden the preheat zone of the flame without affecting the thin reaction zone. Recently, Peters [5] has suggested that this thickened preheat regime should replace a portion of the classical distributed reaction regime. Specifically, eddy penetration into the preheat zone ($\mathrm{Ka} > 1 \Rightarrow \delta_L/\ell_k > 1$) results in enhanced transport of heat and radicals from the reaction zone to the unburned reactants. The limits to the thickened preheat regime are $\mathrm{Re_T} > 1$, $\mathrm{Ka} > 1$, and $\mathrm{Ka}_\delta < 1$, where the second Karlovitz number is based on the thickness of the inner reaction zone, i.e., $\mathrm{Ka}_\delta = (\ell_\delta/\ell_k)^2$. This upper limit implies that the Kolmogorov length scale is larger than the thickness of the inner reaction zone, and thus cannot penetrate into it. Contrastingly, beyond the thickened preheat regime is the classic well-stirred reactor regime, or what Mansour et al. [8] refer to as the broken reaction regime. Here, the turbulence is strong enough to disrupt combustion in the inner reaction layer, which can ultimately result in extinction of the flame.

Recent experimental evidence supports the existence of a thickened preheat regime. Chen et al. [9], for example, provide two-dimensional Rayleigh scattering images for a set of turbulent stoichiometric methane-air jet flames. From their images, locations near the flame front are observed where the distance between temperature iso-contours expands within the preheat zone. This result is explained by small yet energetic eddies entering into and broadening the preheat zone, as hypothesized for the thickened preheat regime [5]. Buschmann et al. [10] and Chen and Mansour [11] present simultaneous two-dimensional temperature and OH measurements (via laser-induced pre-dissociative fluorescence and planar saturated LIF, respectively) in premixed methane-air Bunsen flames (stoichiometric and lean). Depending on the turbulence intensity, different features are found in these scalar images. At low turbulence intensities, locations having large temperature and OH gradients are apparent, consistent with a wrinkled flamelet concept. As turbulence intensity rises ($\upsilon'/S_L = 14$, $\mathrm{Ka} = 5$ in [10]), reduced temperature gradients are observed, thus suggesting thickened preheat zones. However, large OH gradients remain, indicating the simultaneous presence of thin inner reaction zones. At large turbulence intensities ($\upsilon'/S_L = 26$, $\mathrm{Ka} = 13.6$), a local absence of OH is observed in some cases while the temperature remains high (~1500 K) indicating localized extinction. Such extinction events may occur owing to large local strain rates that quench controlling reactions.

The thickness of the CH layer in a flame is much thinner than that of OH, and can thus be used as a more stringent test for the indication of an instantaneous reaction zone. Mansour et al. [8] have reported simultaneous two-dimensional temperature and CH images in the same flames studied by Chen et al. [9]. Their results indicate similar occurrences as those mentioned previously based on simultaneous temperature/OH image measurements [11]. There are again locations containing steep temperature gradients and large CH peaks, corresponding to wrinkled flamelets. There are also locations having smaller temperature gradients, thus providing additional evidence for the existence of a thickened preheat zone ahead of the inner reaction layer. Reduced CH and even the absence of CH are observed in the highest strain rate flame ($\mathrm{Ka} = 91$), specifically at locations for which the temperature gradient indicates localized extinction.

Based on the above work, the goal of the current investigation was to employ picosecond time-resolved laser-induced fluorescence (PITLIF) to study turbulent premixed combustion in the thickened preheat regime. Previous investigations using PITLIF for non-premixed flames [12] has provided solid evidence for the existence of wrinkled flamelets. Therefore, the objective was to determine whether PITLIF time-series measurements could distinguish between flamelet and possible non-flamelet conditions, as hypothesized to exist under some conditions for turbulent premixed flames.

Some flames utilized in this investigation have been extensively studied by Gore and co-workers at Purdue University [13–17]. In particular, measure-

ments of temperature, radiation, and multiple species [13,14], plus velocity and pollutant emission indices [15] have been obtained for these flames. Additionally, modeling of mean temperatures, velocities [16], and radiation [17] have successfully utilized a unique approach based on a joint reaction progress variable and mixture fraction. These turbulent premixed flames provide a substantial database of measured data and modeled results. Furthermore, the specific flames investigated are mainly in the theoretical thickened preheat regime, thus providing an opportunity for utilizing PITLIF to distinguish between temporal statistics of OH for flames with different instantaneous reaction zone structures.

2. Experimental setup and operating conditions

The laser and optical systems are identical to those used by Renfro et al. [12]. Briefly, a mode-locked Ti:Sapphire laser, with an 80-MHz repetition rate and a pulse width of 18 ps, is frequency tripled to a wavelength of 309.33 nm, which excites the Q_1 (8) line within the (0,0) vibrational band of the $X^2\Pi - A^2\Sigma$ electronic system of OH. The incident laser beam is focused to a beam waist diameter of 108 μm. The third dimension of the probe volume is 125 μm, as determined by the monochromator entrance slit and the detection optics. A 0.25-m monochromator filters the OH fluorescence at 309 nm with a 10-nm window. A PMT after the monochromator, in conjunction with a gated photon counting system, permits determination of time series for OH fluorescence lifetime, OH concentration, and background signal. The raw data from the photon counting system is processed using a correction algorithm to account for system nonlinearities and saturation [18].

The burner used for the turbulent premixed methane-air jet flames is identical to that used in previous studies at Purdue [13–17]. The premixed fuel/air mixture exits from a 15-mm inner-diameter tube that is surrounded by a 100-mm diameter air co-flow. The length of the main fuel tube is greater than 30 times its diameter to ensure fully developed turbulent flow. Four-millimeter glass beads are used in the 100-mm annulus to provide a uniform velocity profile for the air co-flow. A hydrogen diffusion flame is used as a pilot for the flames, with the hydrogen issuing from a 90-port burner at a mean diameter of 20 mm. Each pilot port has a diameter of 0.2 mm.

The majority of the data was gathered from six premixed methane-air flames at three equivalence ratios (0.6, 0.7, and 0.8) and two Reynolds numbers (8700 and 17,400) based on cold flow properties at the jet exit. Additional data were also acquired in a Re = 17,400, Φ = 0.55 flame. For all flames, the maximum diameter of the flame brush was ~20 mm. The length of the flame brush for the Re = 17,400 flame at Φ = 0.8 was ~140 mm, with an approximately 15% drop in length at Re = 8700 or for Φ = 0.6. The hydrogen pilot flow rates were originally chosen to minimize pollutant emission indices in the Φ = 0.8 flames [15], and the same pilot flow rates were used in this investigation (2 mg/s and 3.5 mg/s for the Re = 8700 and Re = 17,400 flames, respectively). On average, the pilot accounted for 6–8% of the total flame heat release.

The operating conditions for the turbulent, lean-premixed, methane-air jet flames considered in this study are given in Table 1 along with relevant scales and dimensionless parameters. The mean velocities (U) are determined from the mass flow rates and the area at the jet exit. The rms velocities (u') are those measured by Kelkar [15] in the two Φ = 0.8 flames, 5 mm from the jet exit. The peak measured turbulence intensities in these two flames are 12% and 35%, respectively. The integral length scale (ℓ) was determined by Ji et al. [17] in the Re = 8700, Φ = 0.8 flame by a best fit of spatial and temporal radiation simulations to measured data at a height of x = 40 mm. In their simulations, the integral length scale, ℓ, increased linearly with axial height. By comparison, Chen et al. [9] report an integral length scale of 2.4 mm for a jet diameter of 12 mm at the exit of a similar burner based on velocity measurements. The values of u' and ℓ determined from the Φ = 0.8 flames are used in Table 1 for all the flames under investigation for lack of better information.

The laminar flame speeds in Table 1 are taken from Andrews and Bradley [19]. The values of flame thickness are determined using Eq. 3, and a value for thermal diffusivity (or molecular diffusivity, assuming Le = 1) of 7.0×10^{-5} m^2/s. This value was used by Plessing et al. [20], based on a calculation of λ/c_p given by Smooke [21]. The thermal diffusivity is calculated as $\alpha = \lambda/(\rho_0 \times c_p)$, where λ/c_p is evaluated at a temperature of 1500 K, which is an approximation of the temperature at the inner layer of the reaction zone. The turbulent Damköhler numbers, Reynolds numbers, Kolmogorov scales, and Karlovitz numbers were also determined using this value for the kinematic viscosity and Eqs. 1–5.

The values of u'/S_L and ℓ/δ_L theoretically place the current flames in the thickened pre-heat regime, except for the leanest flames (Φ = 0.55 and Φ = 0.6) at Re = 17,400 (see Fig. 1). The latter flames are in the broken reaction regime, assuming an inner reaction zone thickness one-tenth of the preheat zone thickness ($Ka_\delta = 1$). The turbulent Karlovitz number ranges from 5.78 to 213, or correspondingly, δ_L/ℓ_k

Table 1
Operating conditions and relevant length scales, time scales, and dimensionless parameters for premixed jet flames

Reynolds number	8700	8700	8700	17,400	17,400	17,400	17,400
Φ	0.8	0.7	0.6	0.8	0.7	0.6	0.55
Heat release (kW)	4.56	4.02	3.48	9.11	8.05	6.96	6.41
U (m/s)	9.22	9.22	9.22	18.4	18.4	18.4	18.4
u' (m/s)	1.89	1.89	1.89	7.18	7.18	7.18	7.18
ℓ (mm)	2	2	2	2	2	2	2
S_L (cm/s)	29	22	16	29	22	16	13
δ_L (mm)	0.241	0.318	0.438	0.241	0.318	0.438	0.538
ℓ/δ_L	8.29	6.29	4.57	8.29	6.29	4.57	3.71
u'/S_L	6.52	8.59	11.8	24.7	32.6	44.8	55.2
Re_τ	54	54	54	205	205	205	205
Da_τ	1.27	0.73	0.39	0.33	0.19	0.10	0.07
Ka	5.78	10.0	19.0	42.8	74.3	140	213
ℓ_k (mm)	0.100	0.100	0.100	0.037	0.037	0.037	0.037
v_k (m/s)	0.697	0.697	0.697	1.90	1.90	1.90	1.90
t_k (ms)	0.144	0.144	0.144	0.019	0.019	0.019	0.019
δ_L/ℓ_k	2.40	3.17	4.36	6.54	8.62	11.9	14.6

Measurements and calculations for the various scales and dimensionless parameters are discussed in the text.

ranges from 2.4 to 14.6. Based on order-of-magnitude arguments, the Kolmogorov eddies in all the flames are much smaller than the laminar flame thickness.

Theoretically, the Klimov-Williams criterion, $Ka < 1$, determines the upper limit for the flamelet regime. However, as reviewed by Mansour et al. [8], experiments [9,10], and direct numerical simulations [22] have shown that the flamelet regime may extend up to $Ka = 10$. Therefore, the current flames may actually be split among the corrugated flamelet, thickened preheat, and broken reaction regimes.

Measurements were obtained in a sequence of premixed jet flames at axial locations from 20–250 mm. Radial profiles of mean OH concentration, fluorescence lifetime, and background emission were obtained by averaging at each point over three seconds with a 10-Hz sampling rate. Time series were taken at five or more radial locations along each mean profile by sampling 4096 data points at 16 kHz and 32 kHz for the Re = 8700 and Re = 17,400 flames, respectively. Quantitative OH concentrations were calibrated against a well-characterized lean, premixed flame stabilized on a McKenna burner [12]. Fifty consecutive time series were taken at each location permitting autocorrelation functions and power spectral densities (PSDs) to be averaged, thus resulting in cleaner statistics. Shot noise corrections were performed on the auto-correlation functions as described in Ref. 12. Probability density functions (PDFs) were also calculated for all data in each time-series set.

3. Results

3.1. Time-averaged results

Typical mean [OH] radial profiles are given in Fig. 2 for one of the premixed flames (Re = 8700, Φ = 0.8), which are indicative of the profiles taken in all of the premixed flames. For axial locations $x \leq 60$ mm, the radial location of peak mean [OH], r_p, is relatively constant around 9–10 mm. Farther downstream, the peak approaches the centerline and eventually reaches the centerline at $x \geq 150$ mm. The locations of peak [OH] match well with the measured peak temperature locations [13,14]. Other features apparent from the mean [OH] profiles are a decrease in peak concentration, $[OH]_{max}$, with increasing axial height and an accompanying increase in profile radial width, as discussed below.

Kelkar [15] reports average axial and radial velocity profiles using LDV in the two $\Phi = 0.8$ flames of this study, as well as in similar flames at $\Phi = 1.0$. The axial velocity of the fuel core transitions towards a flat radial profile at locations approaching 100 mm from the jet exit. The sharp radial gradient of the shear layer is located immediately outside this fuel core. Mean [OH] peaks at $x < 100$ mm are located on the reactant side (fuel core side) of the shear layer. For $x \geq 150$ mm, the velocity profiles approach a self-similar shape and the mean [OH] peaks approach the jet centerline. Furthermore, mean equivalence ratio profiles determined from measured species concentrations in the $\Phi = 0.8$ flames [13] indicate that little mixing with co-flow air occurs inside radial

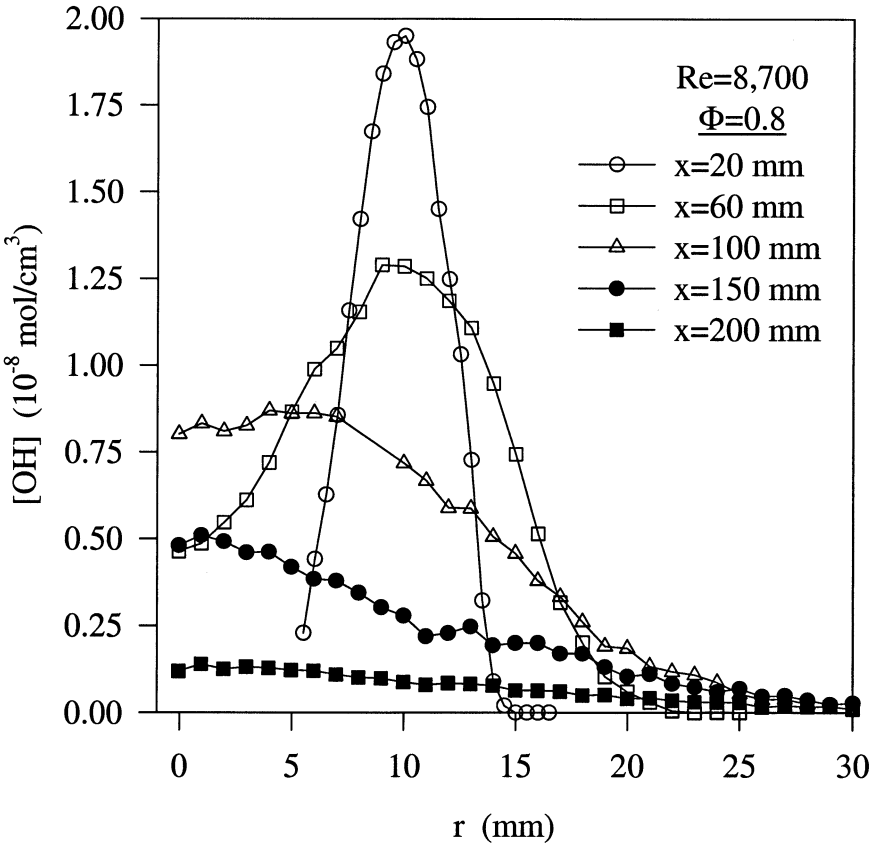

Fig. 2. Time-averaged [OH] radial profiles for the Re = 8700, Φ = 0.8 premixed jet flame. The data were taken with a 10-Hz sampling rate for three-second sampling times at each location. The profiles are quantified by calibration of the peak concentration at x = 60 mm against a known value in a previously quantified laminar flat premixed flame.

locations corresponding to peak temperatures, thus suggesting that complete combustion of the premixed reactants occurs before any entrainment of air.

The mean [OH] profiles from all premixed jet flames can be normalized by employing $[OH]_{max}$, r_p, and the associated full-width at half-maximum (FWHM). The FWHMs are determined by fitting mean radial profiles with a Gaussian curve, which accurately captures the shape of these profiles. The resulting values are given in Table 2 for the different flames at each axial height, while Fig. 3 shows normalized radial profiles at five heights from each of the flames. The resulting collapse indicates that the average normalized distribution of [OH] is the same for each flame at every height for the measured conditions and that differences in the mean OH structure can be characterized by these three parameters. This collapse of mean species profiles was also found in previous work [12,23].

Table 2 indicates a substantial increase in $[OH]_{max}$ from Φ = 0.6 to Φ = 0.7, as expected based simply on the change in stoichiometry. However, an interesting discrepancy arises between equivalent flames at two different Reynolds numbers. Figure 4 presents $[OH]_{max}$ normalized by $[OH]_{max}$ at x = 20 mm versus axial position for the premixed jet flames. The axial decay of $[OH]_{max}$ clearly occurs more rapidly at lower equivalence ratios in the Re = 17,400 case. In particular, the ratio of peak concentrations between x = 20 and x = 200 mm (x/D = 1.33 and 13.3) is 15 for the Φ = 0.6 flame and 5.3 for the Φ = 0.8 flame at Re = 17,400. In comparison, no such dependence between Φ = 0.6 and Φ = 0.8 occurs for the Re = 8700 case. This unique change in premixed flame structure, as determined by mean [OH], may suggest that the dominant reaction-turbulence interaction is different for those flames most strongly within the thickened preheat regime or even within the broken reaction regime. Specifically, the greater axial reduction in $[OH]_{max}$ for the Re = 17,400 flames is consistent with an increased fre-

Table 2
Hydroxyl concentration and fluorescence lifetime statistics at locations of peak $[OH]_{avg}$

Re	Φ	x (mm)	r_p (mm)	FWHM (mm)	$[OH]_{max}$ (10^{-8} mol/cm^3)	$[OH]_{rms}$ (%)	τ_{avg} (ns)	τ_{rms} (%)
8700	0.6	20	9.0	3.3	1.48	26	1.78	8.7
		60	9.0	5.2	0.84	54	1.89	17.3
		100	9.0	8.2	0.65	65	1.93	23.1
		150	5.5	13.1	0.55	75	1.91	22.1
		200	0.0	26.3	0.26	108	1.76	20.8
8700	0.7	20	9.0	4.1	1.79	27	1.80	13.4
		60	9.0	9.2	1.17	41	1.87	16.6
		100	7.5	16.6	1.05	43	1.89	15.2
		150	0.0	27.5	0.66	52	1.69	10.8
		200	0.0	48.9	0.15	93	1.33	23.4
8700	0.8	20	9.5	5.0	1.95	17	1.59	1.7
		60	9.5	12.6	1.29	26	1.78	9.9
		100	0.0	21.9	0.87	32	1.72	11.6
		150	0.0	32.6	0.51	53	1.54	14.0
		200	0.0	35.2	0.14	128	1.40	22.5
17,400	0.55	20	8.5	2.8	1.29	38	1.73	14.3
		40	9.0	4.0	0.52	87	1.74	19.9
		60	8.5	6.3	0.19	158	1.64	24.9
		80	8.0	14.2	0.06	212	1.28	29.6
17,400	0.6	20	8.5	2.9	1.80	41	1.88	10.9
		60	9.0	5.4	0.58	104	1.87	22.2
		100	8.5	8.3	0.28	162	1.75	22.8
		150	0.0	14.6	0.16	184	1.50	22.2
		200	0.0	15.0	0.12	143	1.25	20.3
17,400	0.7	20	8.8	3.5	1.88	25	1.78	5.5
		60	9.3	6.7	1.23	45	1.90	18.4
		100	8.3	11.5	0.93	61	1.91	24.2
		150	3.3	18.2	0.78	65	1.88	22.6
		200	0.0	25.4	0.43	84	1.63	21.5
17,400	0.8	20	9.0	3.9	2.02	22	1.73	8.7
		60	10	8.5	1.42	31	1.85	12.6
		100	8.0	14.2	1.15	42	1.88	18.7
		150	0.0	22.6	0.78	48	1.72	15.7
		200	0.0	27.3	0.38	87	1.45	18.4

FWHMs are determined by Gaussian fits to the mean [OH] radial profiles. $[OH]_{max}$ (10^{-8} mol/cm^3), $[OH]_{rms}$, τ_{avg}, and τ_{rms} are determined from the time series.

quency of local extinction events for highly stretched flames at lower equivalence ratios.

The associated mean [OH] profile widths (FWHM) are described well by a linear relation with axial location between 20 and 150 mm. The mean widths broaden much faster with downstream location at decreasing Reynolds number and as the flames approach $\Phi = 1.0$ (see Table 2). As the equivalence ratio rises, the increased heat release substantially affects the growth of the mean [OH] profiles, particularly at the lower Reynolds number. On the other hand, at $\Phi = 0.6$, the change in Reynolds number results in little difference with respect to the growth of the profile FWHMs. This result suggests that the change in Reynolds number only creates a noticeable difference in the mean [OH] structure if the heat release is sufficiently large.

The $[OH]_{rms}$ values determined from each time series at the location of $[OH]_{max}$ are listed in Table 2, with an appropriate correction for shot noise as described by Renfro et al. [24]. The $[OH]_{rms}$ values are generally significant owing to the intermittency of OH, especially at lower average OH concentrations. A strong correlation between intermittency and $[OH]_{rms}$ has also been observed for turbulent nonpremixed jet flames [12,23]. When calculated conditioned on the presence of OH, the $[OH]_{rms}$ values are nearly constant (~25%).

Mean and rms values for OH fluorescence lifetimes (τ_{avg} and τ_{rms}) are also reported in Table 2. The

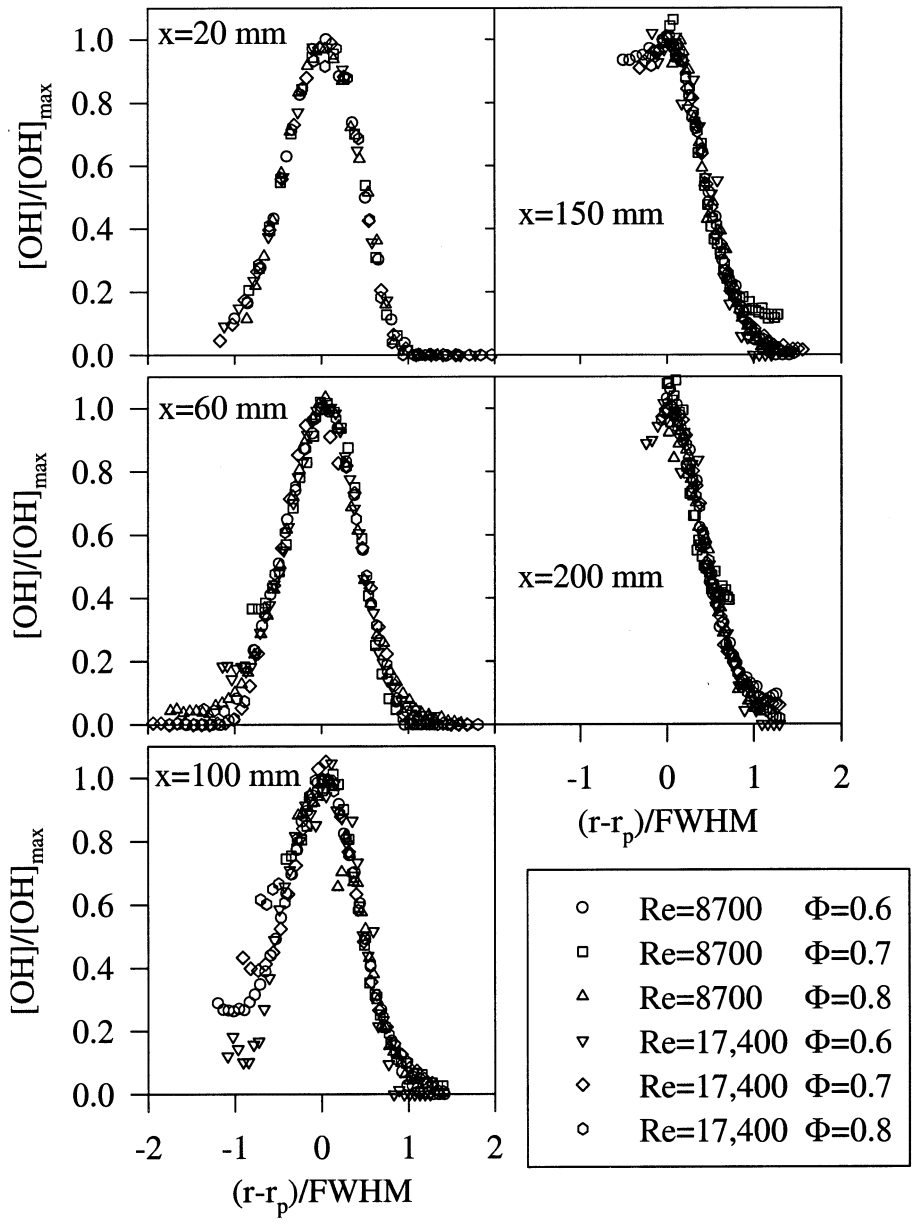

Fig. 3. Time-averaged [OH] radial profiles in six premixed jet flames, normalized by r_p, FWHM and $[OH]_{max}$, as given in Table 2. All profiles collapse to a single curve. The data were taken with a 10-Hz sampling rate for three-second sampling times at each location.

mean lifetimes are nearly constant at a given axial height, changing by no more than 10% in any flame. Hydroxyl quenching depends directly on the concentrations of specific quenching partners and inversely with temperature [25]. Two efficient quenchers of OH are the products H_2O and CO_2. Chakka [13] provides mean H_2O and CO_2 mole fractions along with temperature for the $\Phi = 0.8$ flames. At increasing radial locations, temperatures tend to fall as product species concentrations drop; hence, it appears that these two effects cancel so that the fluorescence lifetimes remain roughly constant. Farther downstream, temperatures diminish rapidly owing to entrainment of co-flow air; thus, the mean lifetime undergoes significant reduction.

3.2. Hydroxyl time series

Typical OH fluorescence time series, obtained in the Re = 8700, $\Phi = 0.8$ flame at x = 60 mm, are

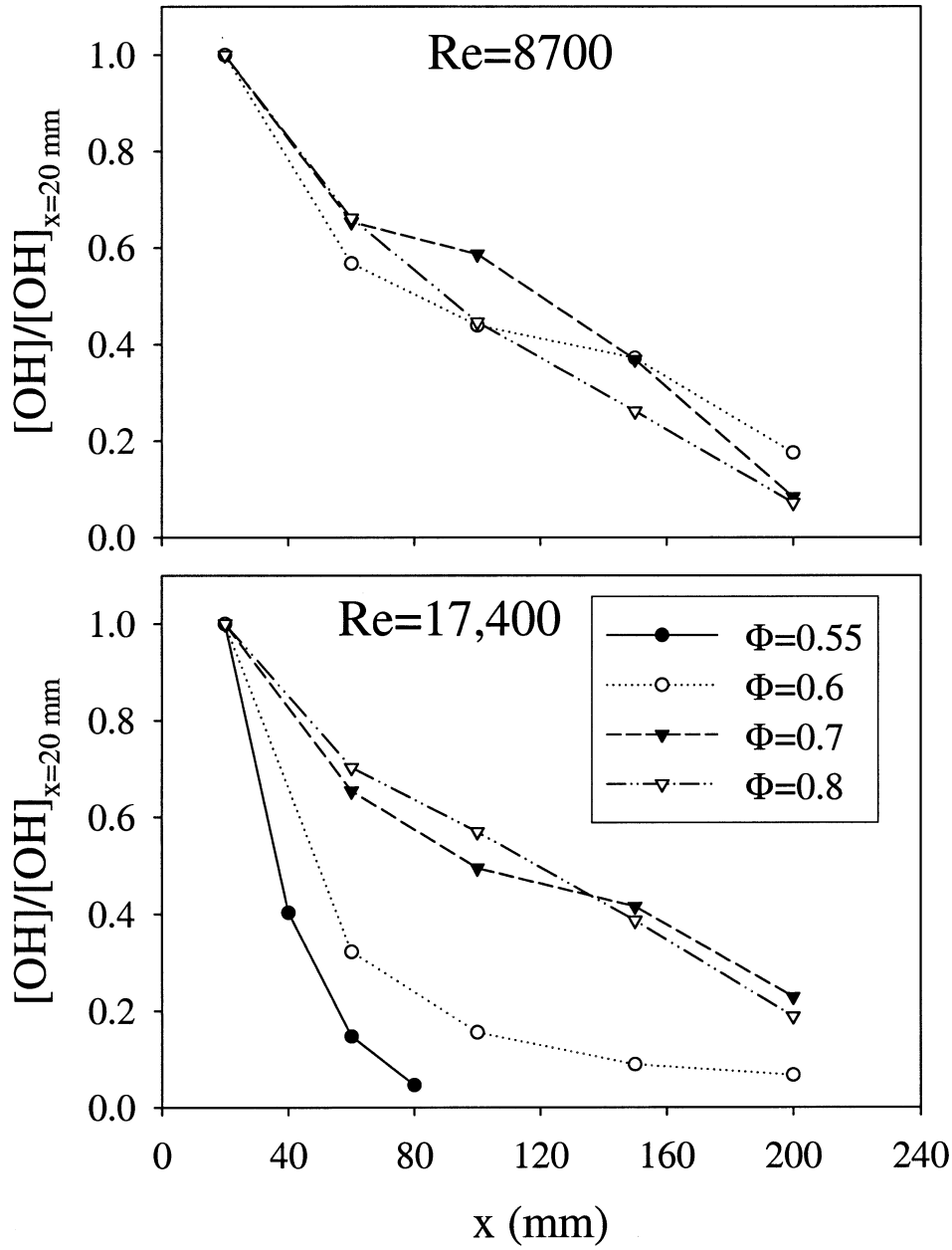

Fig. 4. Peak [OH] versus axial position for the premixed jet flames under investigation. The mean values have been normalized by peak [OH] at x = 20 mm for each flame. Note the relative independence from Φ for the Re = 8700 flames.

shown in Fig. 5. This particular flame is closest to the theoretical corrugated flamelet regime; moreover, the other flames, within the thickened preheat regime, display similar behavior. Some very unique features of these turbulent premixed flames are demonstrated at the three different radial locations of Fig. 5. On the air side (AS) of the mean [OH] profile, an intermittent behavior is present similar to that found in non-premixed flames [12], for which a flamelet concept has previously been employed to model relevant scalar temporal statistics [26].

At the location of $[OH]_{max}$, however, the OH time series displays little or no intermittency. As significant OH can exist in the products of premixed flames, this lack of intermittency probably reflects fluctuations confined between the reaction and post-flame

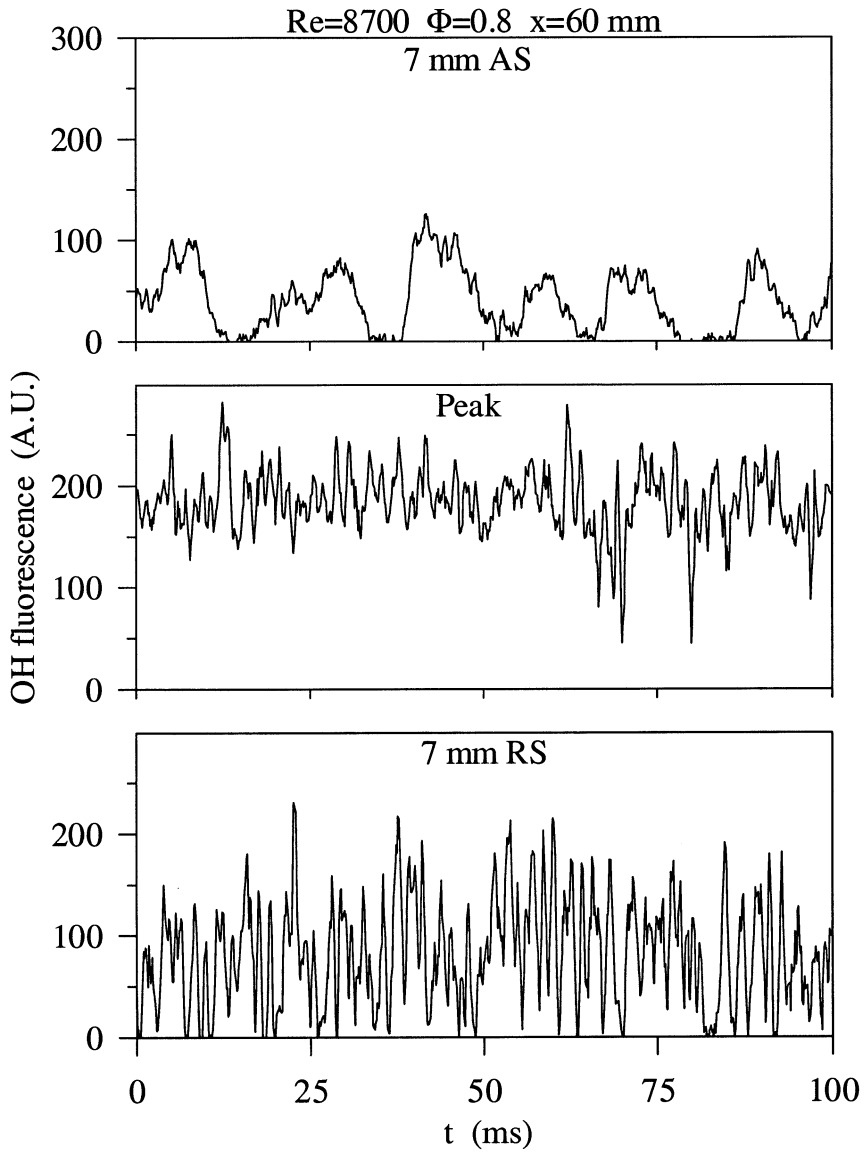

Fig. 5. Hydroxyl fluorescence time series measured in the Re = 8700, Φ = 0.8 premixed jet flame at an axial height of 60 mm. Intermittency is not present at the location of peak [OH]. Note the different fluctuation rates at 7 mm to the air side (AS) and 7 mm to the reactant side (RS) of $[OH]_{max}$.

zones. The measured turbulence intensities for this particular flame are approximately 12% (u'/S_L = 6.52 at x = 5 mm). A similar lack of intermittency is observed in the Re = 17,400 flames, for which the intensities are approximately 35% (u'/S_L = 24.7 at x = 5 mm). At such turbulence levels, we might expect fluctuations to pure reactants or pure air, with no OH, but such behavior is not observed below the flame tip.

Towards the centerline of the burner, into the reactant side (RS) of the mean [OH] profile, we again observe intermittent behavior. However, the time scales at which OH fluctuations occur across the mean profiles at this height are quite different, as is apparent from Fig. 5. The fluctuations at the peak and reactant side of the mean [OH] profiles are much faster than those observed on the air side, consistent with the mean velocity profiles [15]. More importantly, all fluorescence time series obtained at axial heights above the flame tip display an intermittent behavior, similar to that on the air side lower in the flame (see Fig. 5). Here, the only important reactions are probably those responsible for destroying OH.

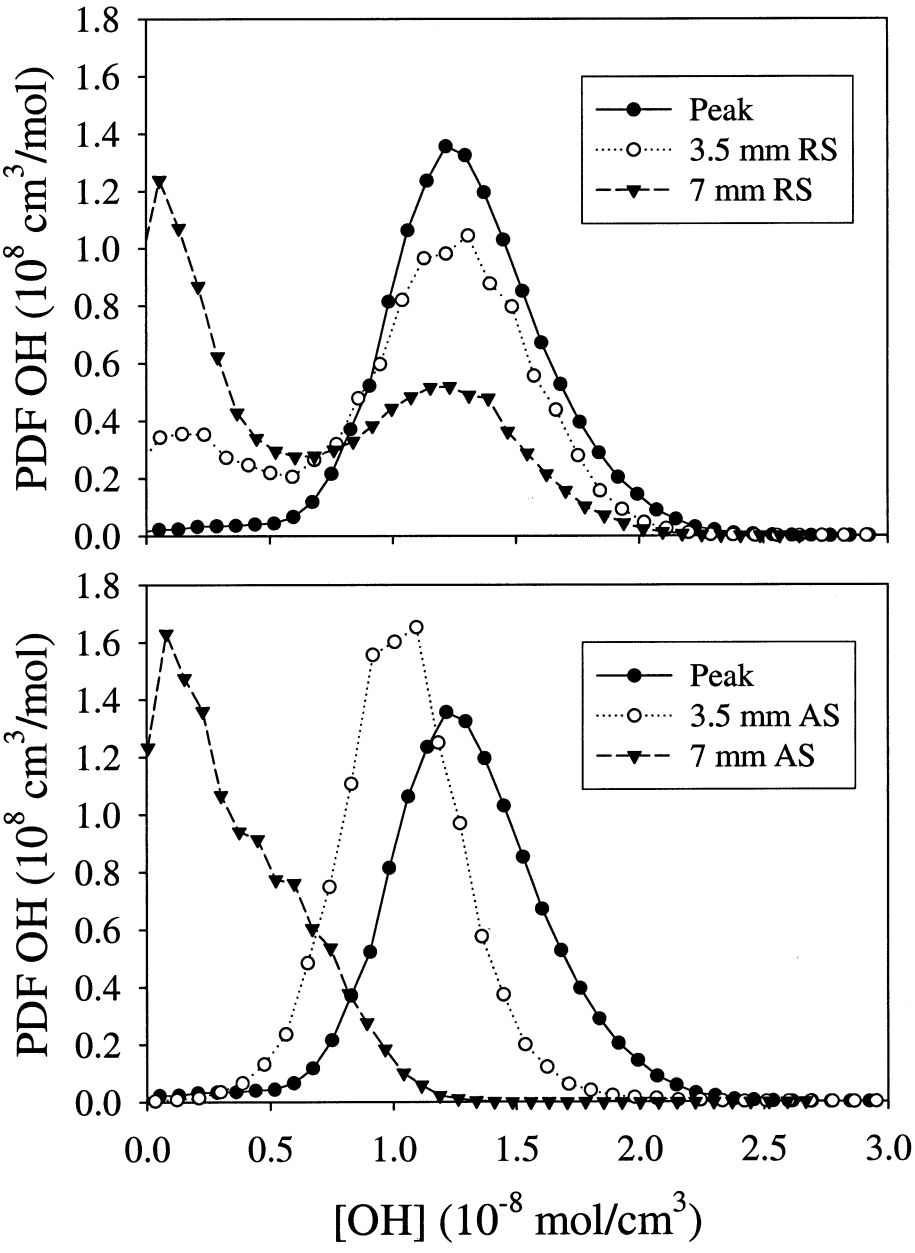

Fig. 6. PDFs for [OH] determined from time series in the Re = 8700, Φ = 0.8 premixed flame at an axial height of 60 mm. The adiabatic equilibrium OH concentration is 0.98×10^8 mol/cm^3, thus indicating super-equilibrium levels of OH in this turbulent premixed flame.

3.3. Probability Density Functions

Figure 6 shows corresponding PDFs from the time series shown in Fig. 5. Although no temporal information is carried by the PDFs, they succinctly summarize over 200,000 data points accumulated at each location where time series were acquired. From PDFs obtained at the locations of $[OH]_{max}$ and to the reactant side (RS), it appears that the distribution of [OH] is almost identical so that OH intermittency determines the mean OH concentrations. This behavior has been observed previously in non-premixed jet flames, except that it occurred across the entire mean [OH] radial profile [12]. In those flames, it was concluded that wrinkled flamelets with relatively constant internal OH structures were present and that the intermittency based on the presence of OH could be

used to explain differences in absolute probabilities for similar [OH] PDFs. The similarity in behavior here could imply that regions near the fuel core, across the mean reaction zone of the current premixed flames, might also be described by wrinkled flamelets, or by some other reaction front providing a constant internal OH structure convected by the turbulent flow field. In fact, Prasad et al. [16] have used various flame surface density models to predict mean temperatures and velocities for this burner between the distributed reaction and laminar flamelet regimes (Re = 7000, Φ = 1.0). Such models are based on the assumption that the reactions occur in many thin sheets analogous to laminar flames, although these sheets are not necessarily continuous in nature.

The air-side PDFs farthest from $[OH]_{max}$ in Fig. 6 have distributions shifted towards lower [OH] values. This feature is indicative of mixing of OH from combustion products with the surrounding co-flow air. For the Φ = 0.8 flames, mean local equivalence ratios at the extreme air-side locations where OH data were acquired at this height are 40–50% lower than at the centerline location [13]. At remaining locations, the mean measured equivalence ratios are no more than 15–20% lower. Hence, enhanced mixing at extreme locations results in shifted distributions of [OH], presumably as OH present in the combustion products mixes with co-flow air. Prasad et al. [16] have previously incorporated a joint PDF of progress variable and mixture fraction to account for this co-flow entrainment.

The most probable values of [OH] found in the PDFs above the flame tip are very similar across their radial profiles, although a shift towards lower [OH] is apparent at farther air-side locations. This behavior correlates with the essentially constant peak fluorescence values observed in the time series. Therefore, the measured [OH] fluctuations are probably dominated by convection, with the mean OH concentrations depending only on the intermittency of any remaining OH. The fact that these locations are above the mean reaction zone also implies that the majority of local OH reactions are slower three-body recombination reactions, as discussed by Barlow et al. [27].

3.4. Temporal statistics for OH

While PDFs characterize the distribution of [OH], autocorrelation functions and PSDs conveniently summarize the relevant temporal statistics. The autocorrelation functions and PSDs are determined from the fluorescence time series, and not from the calculated concentration time series. The temporal statistics obtained from the fluorescence time series display the same information as those from the concentration time series, but with considerably less noise. Therefore, the temporal statistics of the concentration fluctuations are captured adequately by the fluorescence fluctuations. This procedure is justified by the relatively small lifetime fluctuations (τ_{rms}), as given in Table 2 [12,24]. The autocorrelation functions and PSDs have all been corrected for random shot noise, as described by Ref. 24.

Figure 7 shows autocorrelation functions representative of those found in all the premixed jet flames. There are three characteristic shapes depending on the location in the flames. Lower in the flames ($x < 100$ mm) on the air side of $[OH]_{max}$, smoothly decreasing autocorrelation functions exist with strong periodic elements (x = 60 mm, r = 14.5 mm in Fig. 7). This periodicity represents a frequency of about 50 Hz at Re = 8700 and of about 100 Hz at Re = 17,400. The periodic element thus appears to be an artifact of the mean stream flow related to a convective instability. Autocorrelation functions with periodic elements have also been observed for [OH] time-series in non-premixed flames [12], as well as for concentration measurements in non-reacting jets [28], both very near the jet exit ($x/D < 2$). However, for these premixed flames, the periodic element is substantial up to x/D = 7.

On the reactant side of $[OH]_{max}$, the autocorrelation functions display two characteristic decay times (x = 60 mm, r = 4.5 mm in Fig. 7). Here, a sharp initial decrease is followed by a long, slowly decaying tail. Similar [OH] autocorrelation functions have been observed in non-premixed flames [12], but only near the jet exit. They have generally been attributed to laminar effects, as the [OH] layer resides outside the fuel core for non-premixed flames. However, the multi-shaped autocorrelation functions for the current premixed flames occur on the reactant side (fuel core side) of the shear layer at $x/D \leq 7$. The reason for this behavior is currently unknown, although contributions could occur from both turbulent and reaction rate fluctuations.

Chen et al. [9] found that mixing in premixed flames is greatly reduced because of the flame. This observation is consistent with mean equivalence ratio plots for the two Φ = 0.8 pre-mixed flames [13], which show that virtually no mixing occurs within radii corresponding to the peak temperatures until above the flame tip. From the mean velocity profiles [15], the reduced mixing also results in a stronger shear layer, in the form of steeper velocity gradients at extended axial locations. Therefore, we conclude that these uniquely shaped autocorrelation functions are found at larger axial heights for premixed ($x/D \sim 7$) as compared to non-premixed flames ($x/D \sim 2$) owing to a straight-forward extension of near field effects for this jet flow.

At locations higher in the flame ($x \geq 150$ mm), a nearly universal autocorrelation function is apparent

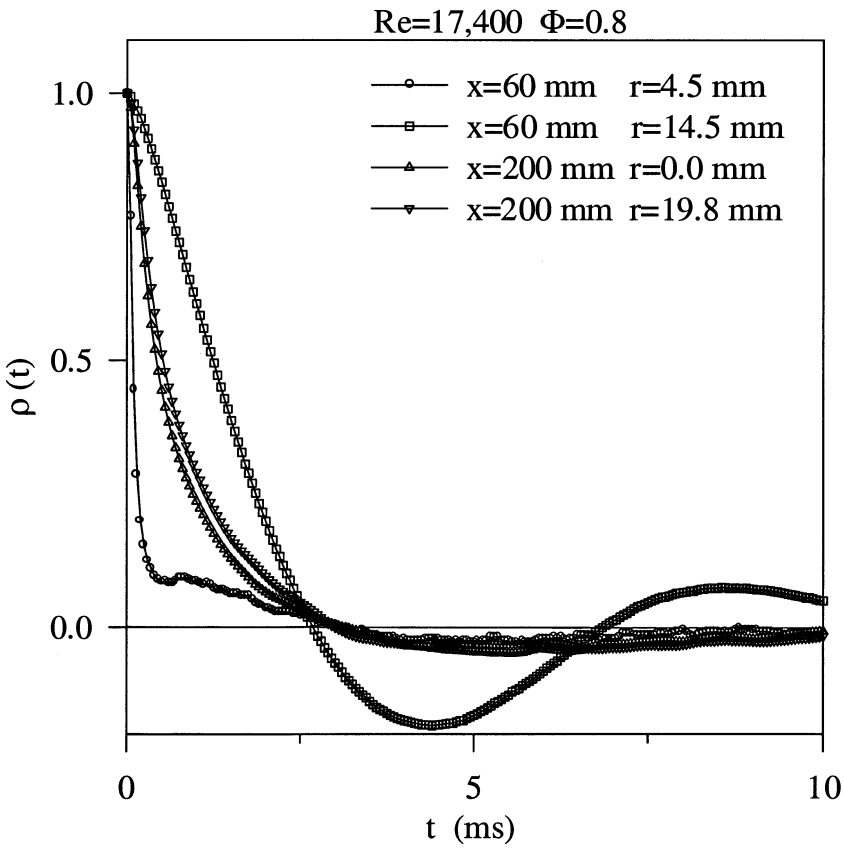

Fig. 7. Typical autocorrelation functions found in the investigated premixed jet flames, taken from the Re = 17,400, Φ = 0.8 case. Note the three distinct shapes, and the effect of radius at the two different axial locations.

(x = 200 mm in Fig. 7). These autocorrelation functions display a simple, nearly exponential decay, typical of the majority of those found previously in non-premixed flames [12]. From Fig. 7, the [OH] autocorrelation functions are very different at x = 60 mm when taken 5 mm to the air side and to the reactant side of the $[OH]_{avg}$ peak. At x = 200 mm, however, the two autocorrelation functions taken 20 mm apart are nearly identical. These trends occur in all of the premixed flames of this investigation.

Figure 8 gives the PSDs for the same conditions as the autocorrelation functions of Fig. 7. As expected, three distinct shapes are noticeable for the different locations throughout the flames. The PSDs at x ≥ 150 mm contain a low-frequency region where the energy content is constant. Above a certain cutoff value, the PSDs display a smooth roll-off, with slopes reaching magnitudes as large as 3.5 at the highest frequencies. No constant-slope regions indicative of an inertial subrange appear to exist in these PSDs. Comparable slopes have been observed for velocity [29] and density [30] PSDs at locations towards the product side of the mean reaction zone. These temporal statistics are probably dominated by velocities conditioned on heat release within the reacting flow [29,30].

On the air side of $[OH]_{max}$ at lower heights, the periodicity observed in the autocorrelation functions is present as a local peak in the spectrum immediately before the high-frequency roll-off region. The slopes of these PSDs in the 100–500 Hz frequency range vary from about −1.5 to −2.5. On the reactant side of $[OH]_{max}$, two distinct time scales are prominent as the PSDs display a very broad elevation in low-frequency content. This low-frequency region roughly extends up to 50 Hz and 100 Hz in the Re = 8700 and Re = 17,400 flames, respectively, where a peak occurs for the air-side PSDs. For lean methane-air V-flames, Gouldin and Halthore [31] report density PSDs that display a similar increase in low frequency content. No clear reasons are apparent for the shapes of these PSDs and for the increase in low-frequency content of the fluctuations.

Integral time scales, τ_T characterizing the fluctu-

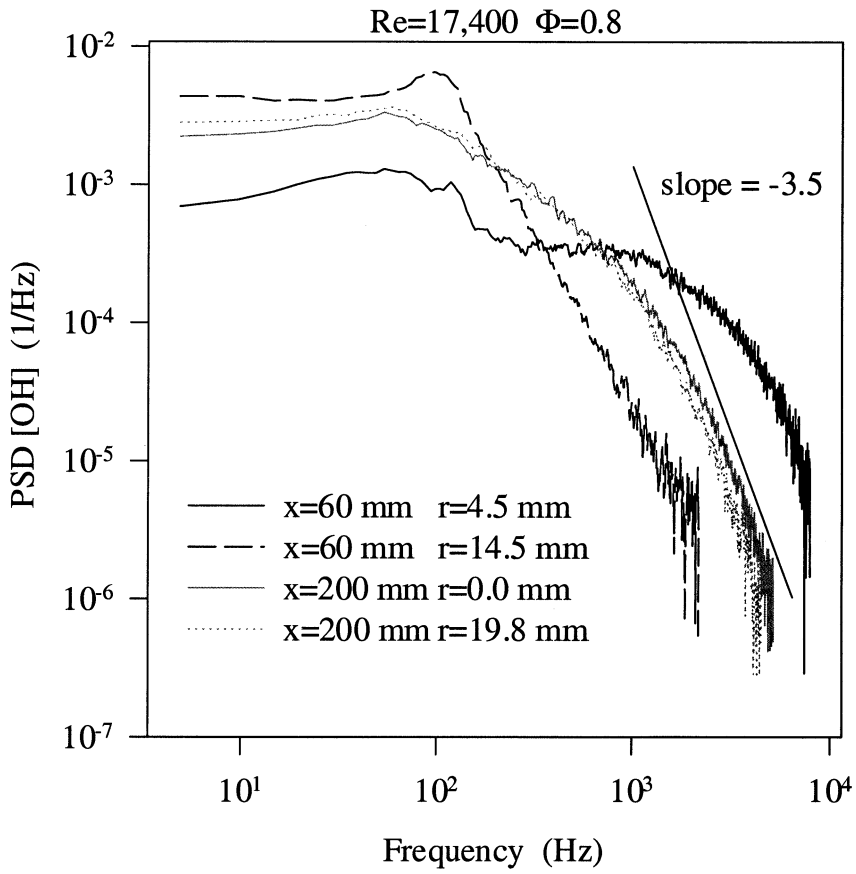

Fig. 8. PSDs for [OH] determined from the time series in the Re = 17,400, Φ = 0.8 premixed jet flame, at the same locations as the autocorrelation functions shown in Fig. 7.

ation rates of [OH], can be calculated by integrating over the autocorrelation functions. Determining a meaningful integral time scale, however, is complicated by the non-exponential shapes of the autocorrelation functions lower in these flames. For example, the absolute value of τ_I obtained from the autocorrelation functions with periodic features depends on the integration window. Fortunately, when varying the length of an integration window, the integral time scales display the same trends, only differing in absolute value. The currently reported τ_I values are determined by fitting an exponential to the first 200 points of each autocorrelation function, so that the abscissa of Fig. 7 is reached in every case. This procedure accurately captures the integral time scales for the exponential autocorrelation functions. The method also provides a single representative time scale for the nonexponential autocorrelation functions, although it is implicitly assumed that these time scales do not capture fully the temporal statistics of their respective time series.

Integral time scales are shown in Fig. 9 for three Re = 17,400 flames at different equivalence ratios. At most heights where data was taken, τ_I tends to decrease from Φ = 0.6 to Φ = 0.8. At x = 150 and x = 200 mm in the Re = 8700 flames, the opposite trend occurs. Very near the jet exit at x = 20 mm, the apparent change in τ_I with Φ at a given radial location is better described as a shift in location of OH. Gagnepain et al. [32] obtained LDV measurements in similar flames both conditioned and unconditioned on the presence of unburned reactants by seeding with olive oil and zirconium oxide, respectively. The unconditioned turbulent kinetic energy was found to increase more rapidly when plotted versus the mean progress variable as compared to the turbulent kinetic energy conditioned on the fuel stream. They concluded that the intermittency of the flame zone affects turbulent fluctuations. A reduction in the unconditioned turbulent kinetic energy was also observed as the equivalence ratio increased from 0.65 to 0.8. Hence, it is possible that the OH integral time scales

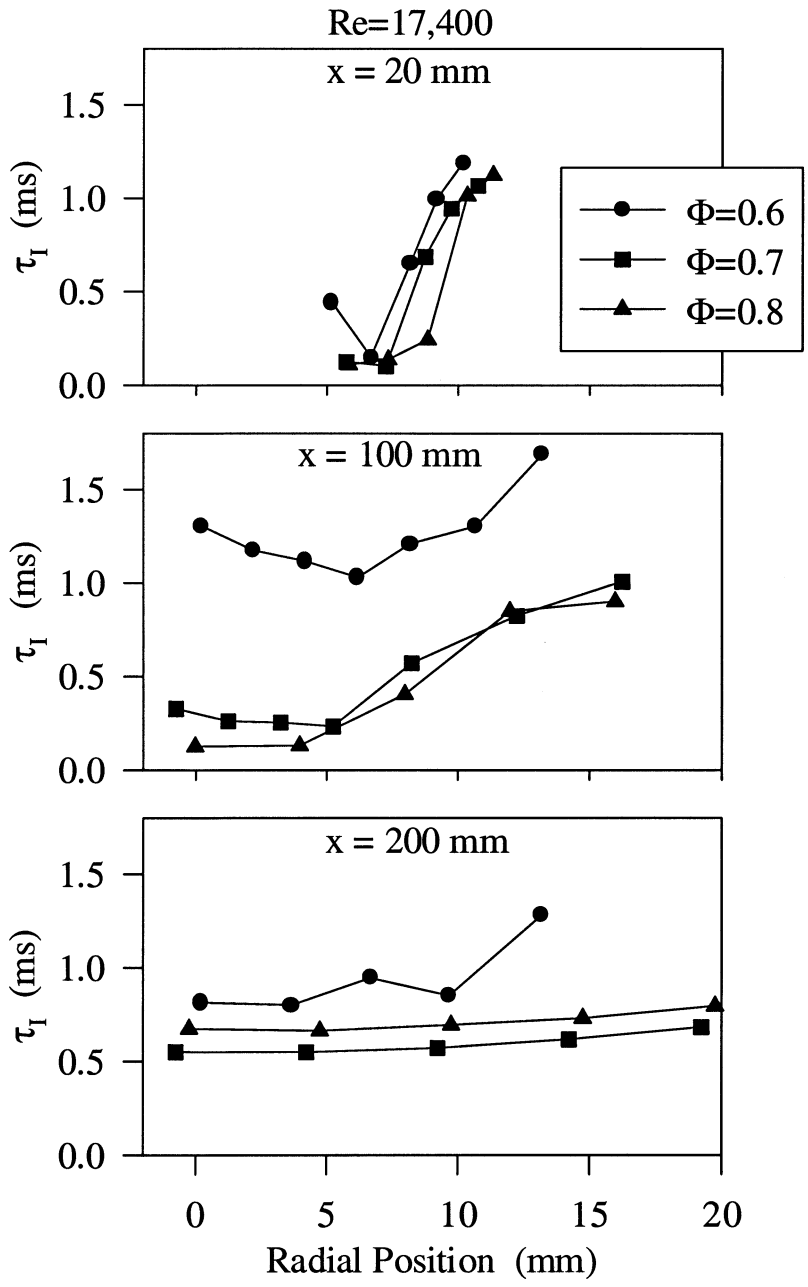

Fig. 9. Calculated OH integral time scales from the measured time series in the Re = 17,400 premixed flames. The time scales were determined by fitting an exponential to the first 200 points of each autocorrelation function.

may be affected by global stoichiometry in part because of a change in turbulent velocity statistics.

Gagnepain et al. [32] also present density and velocity integral time scales at lower Reynolds numbers (~2400 and ~3600) and find a dependence on equivalence ratio similar to that shown here for OH integral time scales. However, the sensitivity of their integral time scales to Φ is smaller at larger Reynolds numbers. Boukhalfa and Gökalp [30] obtained density time series in similar lean premixed methane-air flames. They found that their scalar integral time scales were independent of stoichiometry at Re = 10,000 ($0.7 \leq \Phi \leq 1$), but depended strongly on cold flow characteristics. These results imply a convoluted

influence of both stoichiometry and turbulence on the scalar temporal statistics. Concerning the current premixed flames, a persistent effect of equivalence ratio on integral time scale occurs for both Reynolds numbers. However, as indicated by the mean axial profiles of Fig. 4 and the profile widths, the global structure of the flame is also changing, i.e., the overall flame length and possibly the entrainment rate.

Figure 9 indicates that the integral time scales low in the flame rise sharply from the reactant side to the air side of $[OH]_{max}$ corresponding to the differences noted in the autocorrelation functions of Fig. 7 and the PSDs of Fig. 8. In particular, the τ_I values increase radially by a factor of ~10 in all flames at x = 20 mm, with the relative increase becoming smaller farther from the jet exit. This rapid increase in τ_I for OH has been observed previously in non-premixed flames, but was limited to a factor of three at all axial locations [12]. From the velocity profiles in the Φ = 0.8 flames [15], mean axial velocities decrease by approximately a factor of eight across the radial locations where OH data were collected at x = 20 mm. Hence, the OH fluctuation rates lower in the flames appear to be dominated by mean convection velocities across the reaction zone. Barlow et al. [27] estimate the time scale for OH bimolecular production reactions to be approximately 20 μs, much faster than the time scales presented here. This discrepancy suggests that fluctuations in OH owing to unsteady reaction rates can be de-coupled from convection-dominated fluctuations of existing OH.

Because of their similar shapes, the autocorrelation functions for all flames at x $\geq$ 150 mm collapse when their time axes are scaled by their respective integral time scales. Figure 10 shows some of these autocorrelation functions and their corresponding collapse upon appropriate normalization. Here, the integral time scales among flames are separated at most by a factor of three. This result implies that the distribution in [OH] fluctuations is similar at all downstream locations and can be quantified simply through the integral time scale. Self-similarity at these locations suggests the possibility of determining scaling laws for τ_I as a function of position (r,x) and cold flow characteristics (Re). On the other hand, residual effects of heat release on integral time scales might also prove significant, as discussed previously.

The OH integral time scales are nearly constant across the entire width of the flow at downstream locations (x $\geq$ 150 mm), above the mean flame brush tip. For the Φ = 0.8 flames, the velocities at the greatest radial locations where OH data were taken are roughly 50% of the corresponding centerline velocities [15]; therefore, traditional turbulent scaling based on a mean convection velocity does not apply for these OH integral time scales. Mean equivalence ratio plots [12] show that air entrainment has reached the jet centerline at these downstream locations in the Φ = 0.8 flames. Consequently, the only reactions relevant to OH are the slower three-body recombination reactions. Barlow et al. [27] estimate a time scale for these reactions on the order of 3 ms, which is comparable to an integral time scale at these locations. Hence, the finding that integral time scales are independent of radial location, and thus mean convection velocity, may be a result of opposing effects between turbulent convection and turbulence-chemistry interaction for relevant three-body OH destruction reactions.

A decrease in τ_I for x/D $\geq$ 10 (x $\geq$ 150 mm) is typically observed in all flames. These locations correspond to decreasing temperatures [13] and are thus considered to be above the mean reaction zone. The reported density integral time scales of Gagnepain et al. [32] were measured with respect to a mean axial progress variable, $\langle c \rangle$, as determined from reactant and product passage times. These time scales drop with increasing mean progress variable (axial location) above $\langle c \rangle$ = 0.2, but the associated trend of a smaller integral time scale with increasing axial distance is opposite to that expected from typical turbulent scaling. However, with a decreasing axial temperature, the influence of three-body recombination reactions becomes stronger, as the reaction rates roughly depend inversely on the square of temperature [33].

To determine the effect of jet velocity on the OH integral time scales, 10 time-series were obtained along the jet centerline for Φ = 0.8 at x = 150 mm, with flows ranging from U = 6.9 m/s to U = 24.9 m/s (Re = 6500 to 23,500). This axial position ensures that the location of $[OH]_{max}$ is at the jet centerline for all flames. For these conditions, the autocorrelation functions displayed self-similarity and could be collapsed onto to a single curve as shown in Fig. 10. The resulting τ_I are plotted in Fig. 11, with an observed $U^{-2.12}$ dependence. This dependence on velocity is stronger than that reported for non-premixed flames [12], or that expected for non-reacting turbulent flows based on mean velocity scaling. However, this result could be compromised by a near-field effect or a shift in virtual origin, as the near field in premixed jet flames apparently extends downstream via a reduction in turbulent mixing.

3.5. Time-series modeling

The measured OH time series for turbulent premixed methane-air flames suggest that the mechanisms responsible for the production and destruction of OH in such flames may be modified by high turbulence intensities, although the temporal statis-

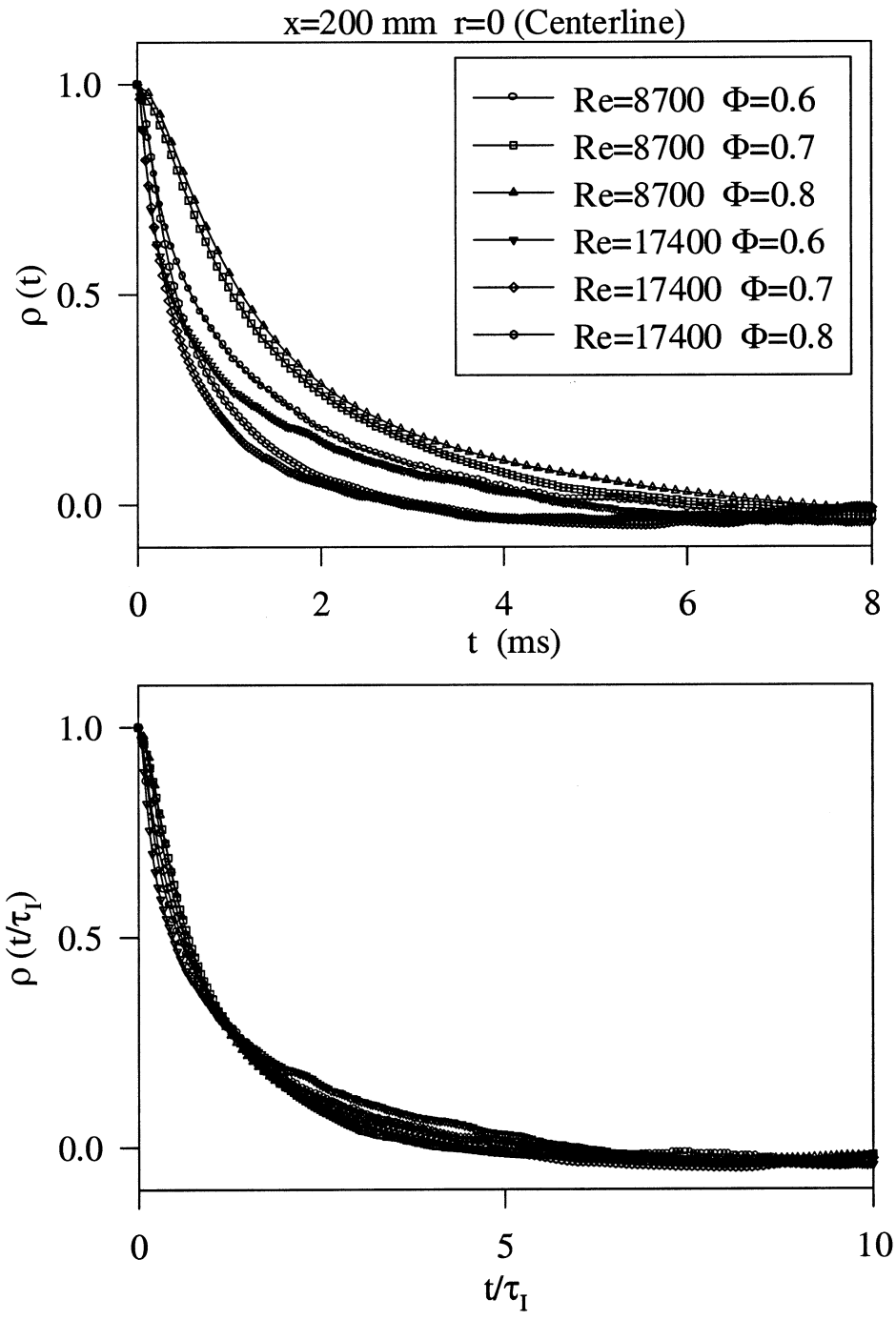

Fig. 10. Autocorrelation functions measured in all six premixed flames at an axial location of x = 200 mm. These autocorrelation functions are typical at x ≥ 150 mm and collapse to a single curve when scaled by their respective integral time scales.

tics appear unaffected. We now pursue further understanding by modeling mean OH profiles and OH integral time scales in turbulent premixed flames through the use of temperature time-series simulations and various temperature-hydroxyl state relationships. In particular, a comparison is made between simulated and measured OH results corresponding to the Re = 8700, Φ = 0.8 case.

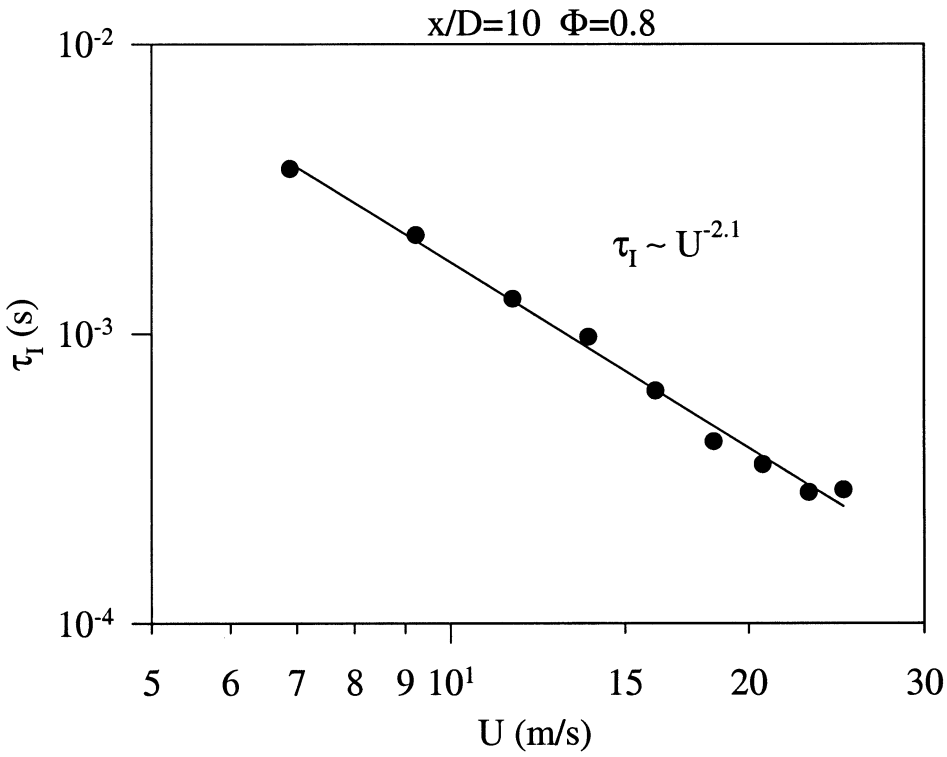

Fig. 11. Integral time scales for OH determined from flames with Re = 6500 to Re = 23,500 at Φ = 0.8. The measurement location was fixed along the centerline at x = 150 mm (x/D = 10).

Equivalence ratio measurements in the same flame [13,16] indicate that the reaction is essentially completed before mixing can occur with co-flow air. Therefore, the reaction zone can be described by a reaction progress variable, while a mixture fraction can be employed beyond the peak temperature based on hot products mixing with cooler entrained air; hence, OH can be jointly mapped via a combined progress variable and mixture fraction. This joint PDF approach was previously employed to predict mean temperatures and velocities for the same burner at Φ = 1.0 using various flame surface density models [16].

In the same vein, Ji et al. [17] have hitherto utilized a stochastic temperature time- and space-series simulation with a combined reaction progress variable and mixture fraction to predict radiation measurements in turbulent premixed flames [17]. Specifically, mean and rms, line-averaged radiation measurements were simulated by using measured mean and rms temperatures, plus CO_2 and H_2O concentrations. Ji et al. [17] also assumed exponential autocorrelation and cross-correlation functions, with prescribed integral length scales at each height and integral time scales determined by utilizing Taylor's hypothesis and mean velocity measurements [15,16].

In general, the simulation procedure began by invoking radial profiles for temperature at each height at an initial instant in time. Temperature profiles and fluctuations were then advanced in time and space by applying assumed autocorrelation and cross-correlation functions. Additional random elements were subsequently introduced to reproduce experimental rms values while measured mean values were invoked to give the correct mean profile shapes. The resulting temperature space-time series gave excellent agreement with measured radiation time series. On this basis, for the current modeling, temperature time series are simulated using the same formulation, while OH time series are created by applying two-dimensional progress variable and mixture fraction state relationships, as described below. Further details on the procedures for creating temperature space-time series can be found in Ji et al. [17].

3.6. State Relationships

Four OH state relationships were examined by employing the one-dimensional, opposed-flow lami-

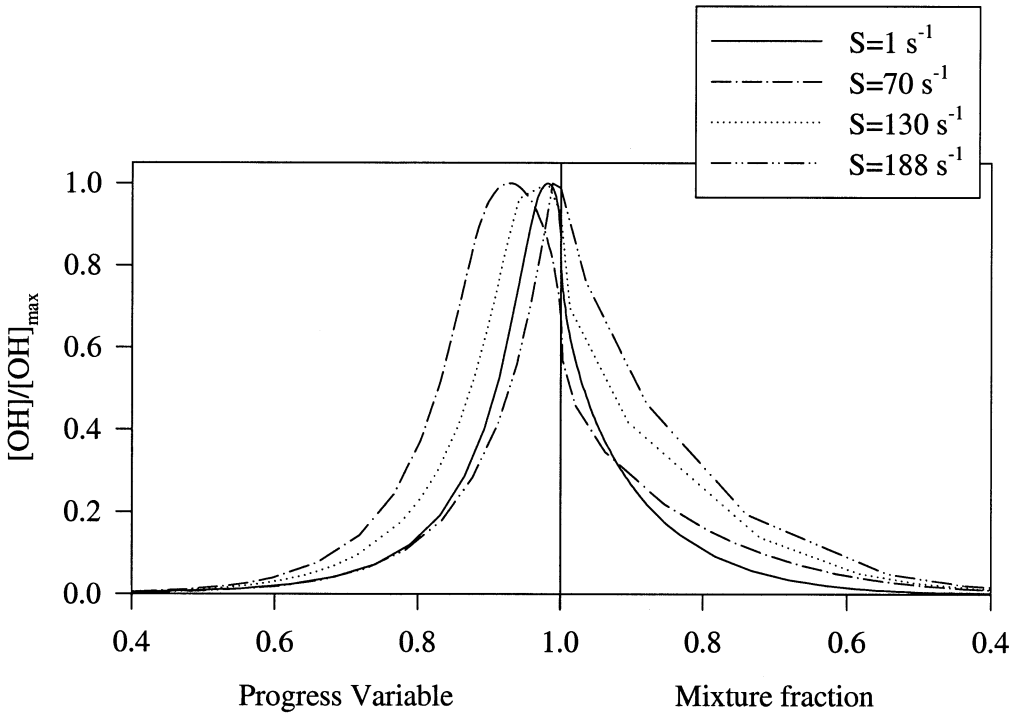

Fig. 12. State relationships between OH and the reaction progress variable and mixture fraction at various strain rates determined from OPPDIF [34] with GRI-Mech 3.0 [33].

nar flame code OPPDIF [34], using GRI-Mech 3.0 [33] and considering gaseous radiation [35]. The input conditions for OPPDIF consisted of premixed methane-air reactants ($\Phi = 0.8$) at 300 K impinging on pure air at 300 K, with strain rates varying from $S = 1\ s^{-1}$ to $S = 188\ s^{-1}$ (the predicted extinction limit). In this manner, the OPPDIF code can be used to predict the flame structure for a premixed turbulent flame. The state relationships are presented in Fig. 12 in terms of a temperature-based progress variable and the mixture fraction for four OPPDIF cases. Because mixing is superfluous before the post-flame region [13], the progress variable is defined only for pure reactants ($\Phi = 0.8$) for which the mixture fraction is unity. The combined state relationship plot represents the structure of OH across the predicted laminar flame, where $c = Z = 1$ defines the instantaneous flame surface (complete combustion with no mixing). In general, the different strain rates result in different peak [OH], different widths in the state relationships, and different locations where the peak OH occurs with respect to the progress variable.

3.7. Simulation Results

Predicted mean [OH] radial profiles, normalized by $[OH]_{max}$, are shown in Fig. 13 for the four strain-rate cases along with a measured mean [OH] radial profile at $x = 40$ mm for the $Re = 8700$, $\Phi = 0.8$ flame. A measured integral length scale of 2 mm was used at this axial height, while integral length scales of 4 mm and 8.5 mm were used at $x = 60$ mm and $x = 100$ mm, respectively [5]. The locations of predicted $[OH]_{max}$ and the profile widths depend on the strain rate utilized in the simulations, directly corresponding to the changes shown in Fig. 12. At $x = 40$ mm, the simulated profile for the largest strain rate ($S = 188\ s^{-1}$) matches the measured data on the air side (mixing side) of $[OH]_{max}$. A similar match occurs at greater heights ($x = 60$ mm and $x = 100$ mm) for a strain rate $S = 130\ s^{-1}$. However, on the reactant side of $[OH]_{max}$, the predicted profiles never approach the measured profiles no matter what strain rate is employed.

These mean profiles indicate that the laminar flamelet approximation, as modeled by OPPDIF, accurately captures the effect of mixing residual OH from hot products with ambient air in a turbulent premixed flame. However, the relationship between OH and reaction progress variable based on temperature from the laminar flame code is clearly inadequate for predicting mean [OH] on the reactant side. Figure 13 also displays integral time

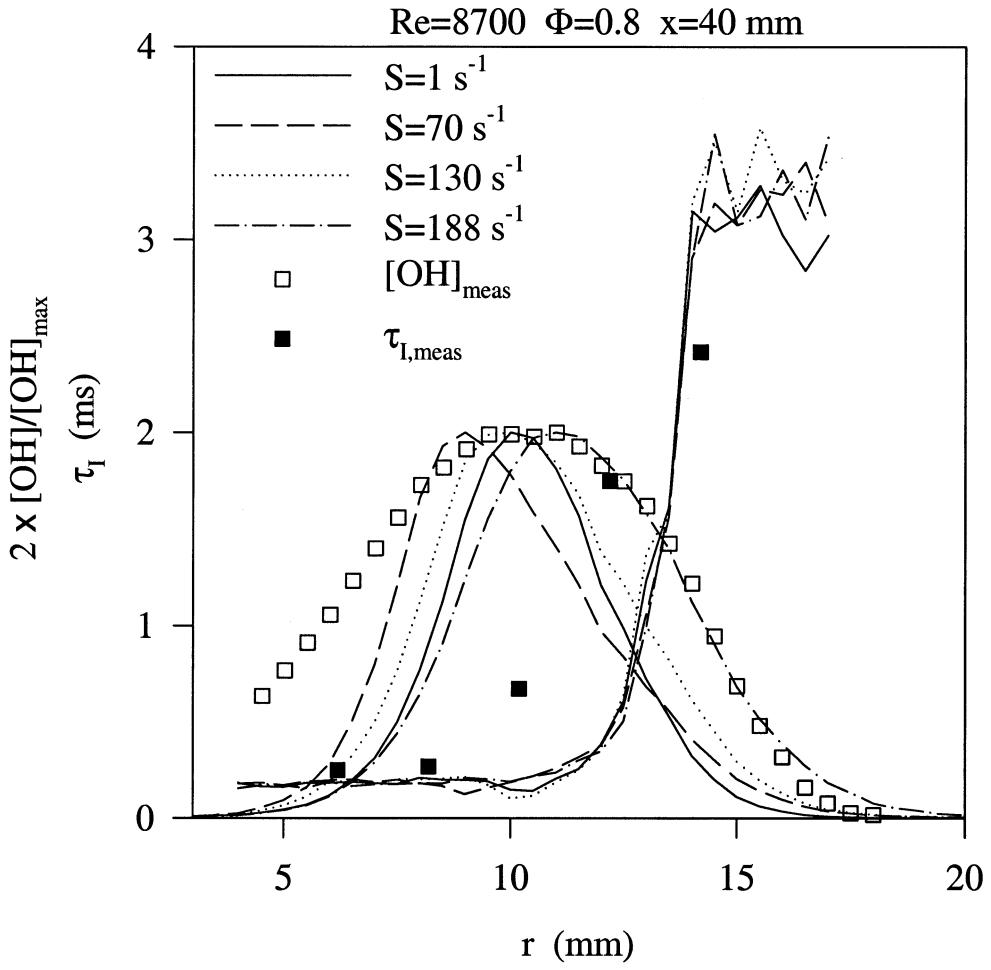

Fig. 13. Measured and predicted time-averaged [OH] radial profiles and integral time scales (τ_I) at x = 40 in the Re = 8700, Φ = 0.8 premixed jet flame. Different strain rates employed in the OH(c, Z) state relationships vary the position of $[OH]_{max}$ and the widths of the predicted mean profiles. The predicted integral time scales are insensitive to the strain rate used to determine the OH(c,Z) state relationships.

scales predicted using the four different strain rates. The predictions are based on autocorrelation functions derived from the OH time-series measurements. In general, the predicted integral time scales are insensitive to the utilized state relationships. We note, however, that the simulations employ a single state relationship computed for a single strain rate while the strain rate itself fluctuates in any given turbulent flame. The predicted time scale's independence from the chosen strain rate suggests that this inherent simplification does not limit the results found via the simulations.

The predictions shown in Fig. 13 follow input temperature time scales, which were determined based on mean convection velocities at each radial location [15]. As a result, the agreement shown in Fig. 13 confirms the suggested relationship between OH integral time scale and mean turbulent convection at these axial heights. The smallest integral time scales on the reactant side of $[OH]_{max}$ display very similar magnitudes. However, at locations beyond $[OH]_{max}$, the predicted integral time scales tend to be smaller than those measured via PITLIF. A sharp increase in the predicted integral time scale occurs at radial positions farther away from the measured integral time scales, and the rise also appears to be steeper. This divergence between predicted and measured OH integral time scales may arise from an increased contribution of turbulence-induced fluctuations in OH reaction rate, which the model intrinsically ignores.

4. Summary and conclusions

Quantitative OH time-series measurements were obtained for the first time in a series of turbulent lean-premixed jet flames. The premixed flames considered are theoretically in the thickened preheat regime [5], for which the preheat zone is broadened by small energetic turbulent eddies, but the primary reaction zone, where heat release and radical production occur, remains thin. The time-averaged radial profiles of OH concentration in all flames were found to be self-similar in shape when scaled by their respective maximum concentrations, peak radial locations, and full-widths at half maxima. Therefore, differences in mean OH flame structure can be characterized through these parameters.

The effect of varying equivalence ratio and total flow rate in these flames is apparent from the broadening of the mean radial profiles with increased heat release and reduced Reynolds number. The axial decay of absolute OH concentration is reduced with increased heat release (increasing Φ) for the Re = 17,400 flames, but remains relatively unchanged for the Re = 8700 flames, suggesting a difference in the relevant turbulence/hydroxyl interactions. The greater turbulent intensities for the larger Re flames may result in more frequent extinction events, thereby reducing mean OH concentrations. This very rapid axial decay of mean [OH] was not observed in previous non-premixed flames [12]. Mean OH fluorescence lifetimes are invariant at a given axial position, suggesting a radial balance between changes in temperature and concentrations of relevant OH quenching partners. Far downstream, considerable reductions in temperature promote a decrease in fluorescence lifetimes [13].

The fluorescence time series for OH display unique results for turbulent premixed flames. On the air side of the mean [OH] profiles, intermittency appears as a result of mixing residual OH from hot combustion products with co-flow air. However, non-intermittent time series are observed at $[OH]_{max}$, presumably where OH bimolecular reactions occur most frequently. One possible explanation for this behavior is that instantaneous OH occurs in a relatively broad region across the flame-front, as OH concentrations remain significant among the products of premixed flames. However, the spatial distribution of OH towards the preheat side of the flame-front may be affected by turbulent mixing from the thin reaction layer, as postulated from thickened preheat zone theory [5]. Non-intermittent time series were not observed for the diffusion flames of Renfro et al. [12], for which wrinkled flamelets are presumed to dominate. Hence, these results demonstrate an important distinction between the reaction zones of two fundamentally different flames, as observed from the OH time series. Far downstream, the OH time series are again intermittent, but the dominant reactions are slower three-body recombination reactions.

PDFs of OH concentration effectively summarize the evolution in flame structure for the various regions of these premixed turbulent flames. The influence of co-flow entrainment on OH PDFs is apparent from the extreme air-side PDFs. PDFs with similar [OH] distributions manifest themselves at locations near the fuel core. The significant conclusion is that even if these flames exist within the thickened preheat regime, the primary internal structure responsible for OH distributions remains constant across the mean flame brush and thus the absolute concentration of OH depends on the intermittency of this instantaneous flamelet structure.

Autocorrelation functions determined from the [OH] time series display three different characteristic shapes depending on their location in a turbulent premixed flame. On the air side of $[OH]_{max}$, where the majority of heat release occurs ($x/D \leq 7$), the autocorrelation functions display a periodic component and exist at locations corresponding to steep velocity gradients. The periodicity seems to be dominated by instabilities accompanying the mean convective field. Reactant-side autocorrelation functions at $x/D \leq 7$ display two characteristic decay times that are both smaller than those for the air-side autocorrelation functions. However, the source of these two distinct decay times is currently unknown, although contributions could occur from both turbulent and reaction rate fluctuations. At locations farther downstream ($x/D \geq 7$), beyond the main heat-release region of the flames, nearly identical exponential OH autocorrelation functions are observed for all radii at a given axial location. Here, air entrainment has reached the centerline of the turbulent flames [13] so that the mean velocity profiles approach self-similarity [15].

The integral time scales for the turbulent premixed flames at $x/D \leq 7$ appear to be dominated by turbulent convection as they increase rapidly outside the jet fuel core. This result indicates that turbulence does not modify OH reaction rates significantly enough to affect temporal statistics, consistent with the observed PDFs. Downstream, the integral time scales are nearly constant radially, suggesting a competing effect between turbulent convection and turbulence-chemistry interactions for the OH destruction reactions. In general, the integral time scales decrease with increasing equivalence ratio for both Reynolds numbers. This behavior is due in part to a thermal modification of the turbulent convective field, but is also a result of changes in absolute flame

structure and relative measurement locations. The autocorrelation functions at downstream locations collapse in all flames when scaled by their respective integral time scales, indicating a similarity in fluctuation rates. The accompanying integral time scales drop slightly farther from the jet exit and decrease significantly with increasing Reynolds number, with a dependence that is modified by prominent near-field effects caused by heat release and reduced mixing with co-flow air.

Finally, hydroxyl time series for turbulent premixed flames have been synthesized by employing temperature space- and time-series simulations. The simulations employed various state relationships for OH versus reaction progress variable and mixture fraction as modeled by OPPDIF. By proper selection of strain rate, predicted mean OH profiles can be made to match measured mean OH profiles on the air side of $[OH]_{max}$, where mixing occurs with co-flow air. Surprisingly, large OH concentrations occur at much lower temperatures on the reactant side than predicted by the simulations. On the other hand, in agreement with our PITLIF measurements, the simulated integral time scales are dominated by mean turbulent convection, as they roughly follow the input integral time scales.

Acknowledgments

We thank Dr. Jun Ji (Purdue University) for providing the temperature data. This work has been supported by the Air Force Office of Scientific Research, with Dr. Julian Tishkoff as technical monitor.

References

[1] G. Damköler, NACA TM 1112 (1947).
[2] F.A. Williams, in: J.D. Buckmaster (Ed.), The Mathematics of Combustion SIAM, Philadelphia, (1985) p. 97.
[3] R. Borghi, in: Recent Advances in the Aerospace Sciences C. Casci (Ed.), Plenum Press, (1985) p. 117.
[4] N. Peters, Twenty-first Symposium (International) on Combustion, The Combustion Institute, Pittsburgh, (1986) p. 1231.
[5] N. Peters, J. Fluid Mech. 384 (1999) 107.
[6] F.A. Williams, Combust. Flame 26 (1976) 269.
[7] H. Tennekes, J.L. Lumley, A First Course in Turbulence, The MIT Press, Cambridge, MA, 1972.
[8] M.S. Mansour, N. Peters, Y.-C. Chen, Twenty-seventh Symposium (International) on Combustion, The Combustion Institute, Pittsburgh, (1998) p. 767.
[9] Y.-C. Chen, N. Peters, G.A. Schneemann, N. Wruck, U. Renz, M.S. Mansour, Combust. Flame 107 (1996) 223.
[10] A. Buschmann, F. Dinkelacker, T. Schäfer, M. Schäfer, J. Wolfrum, Twenty-sixth Symposium (International) on Combustion, The Combustion Institute, Pittsburgh, (1996), p. 437.
[11] Y.-C. Chen, M.S. Mansour, Exp. in Fluids 26 (1999) 277.
[12] M.W. Renfro, W.A. Guttenfelder, G.B. King, N.M. Laurendeau, Combust. Flame 123 (2000) 389.
[13] R.K. Chakka, Experimental Investigation of Scalar Properties of Piloted Turbulent Lean Premixed Flames. M.S. Thesis, Purdue University, West Lafayette, IN, (1996).
[14] J. Ji, Experimental and Theoretical Study of the Spectral Radiation Characteristics of Lean Premixed Flames. Ph.D. Thesis, Purdue University, West Lafayette, IN (2000).
[15] A.S. Kelkar, Flowfield Statistics and Pollutant Emission Indices of Piloted Turbulent Lean Premixed Flames. M.S. Thesis, Purdue University, West Lafayette, IN (1996).
[16] R.O.S. Prasad, R.N. Paul, Y.R. Sivathanu, J.P. Gore, Combust. Flame 117 (1999) 514.
[17] J. Ji, Y.R. Sivathanu, J.P. Gore, Proc. Combust. Inst. 28 (2000) 391.
[18] M.W. Renfro, S.D. Pack, G.B. King, N.M. Laurendeau, Appl. Phys. B 69 (1999) 137.
[19] G.E. Andrews, D. Bradley, Combust. Flame 19 (1972) 275.
[20] T. Plessing, C. Kortschik, N. Peters, M.S. Mansour, R.K. Cheng, Proc. Combust. Inst. 28 (2000) 359.
[21] M.D. Smooke, in: Lecture Notes in Physics M.D. Smooke (Ed.), Springer Verlag, Berlin, (1991) p. 1.
[22] T. Poinsot, D. Veynante, Theoretical and Numerical Combustion, Philadelphia, PA, R.T. Edwards, 2001.
[23] M.W. Renfro, G.B. King, N.M. Laurendeau, Combust. Flame 122 (2000) 139.
[24] M.W. Renfro, G.B. King, N.M. Laurendeau, Appl. Opt. 38 (1999) 4596.
[25] P.H. Paul, J. Quant. Spectrosc. Radiat. Transfer 551 (1994) 511.
[26] M.W. Renfro, J.P. Gore, N.M. Laurendeau, Combust. Flame 129 (2002) 120.
[27] R.S. Barlow, R.W. Dibble, J.-Y. Chen, R.P. Lucht, Combust. Flame 82 (1990) 235.
[28] A.D. Birch, D.R. Brown, M.G. Dodson, J.R. Thomas, J. Fluid Mech. 88 (1978) 431.
[29] I. Gökalp, I.G. Shepherd, R.K. Cheng, Combust. Flame 71 (1988) 313.
[30] A. Boukhalfa, I. Gökalp, Twenty-second Symposium (International) on Combustion, The Combustion Institute, Pittsburgh, (1988) p. 755.
[31] F.C. Gouldin, R.N. Halthore, Exp. in Fluids 4 (1986) 269.
[32] L. Gagnepain, C. Chauveau, I. Gökalp, Twenty-sev-

enth Symposium (International) on Combustion, The Combustion Institute, Pittsburgh, (1998) p. 775.
[33] G.P. Smith, D.M. Golden, M. Frenklach, et al. GRI Mechanism, version 3.0. http://www.me.berkeley.edu/gri_mech/ (1999).
[34] A.E. Lutz, R.J. Kee, J.F. Grcar, OPPDIF: A Fortran Program for Computing Opposed-flow Diffusion Flames, Sandia National Laboratories Report No. SAND96-8243, (1996).
[35] J.P. Gore, J. Lim, T. Takeno, X.L. Zhu, A Study of the Effects of Thermal Radiation on the Structure of Methane/Air Counter-flow Diffusion Flames Using Detailed Chemical Kinetics. Proc. 5th ASME/JSME Joint Thermal Eng. Conf., San Diego, CA, (1999).